Spatially Resolved Dynamic Correlation in the Vortex State of High Temperature Superconductors

Daniel López,[1,2] W. K. Kwok,[1] H. Safar,[2] R. J. Olsson,[1]
A. M. Petrean,[3] L. Paulius,[3] and G. W. Crabtree[1]
[1]*Argonne National Laboratory, Materials Science Division, Argonne, Illinois 60435*
[2]*University of Illinois at Chicago, Chicago, Illinois 60607*
[3]*Western Michigan University, Kalamazoo, Michigan 49008*
(Received 30 September 1998)

We report transport measurements in the mixed state of $YBa_2Cu_3O_{7-\delta}$ single crystals using a contact geometry which enables control of the gradient of the Lorentz force acting on the vortices. The spatial dependence of the vortex velocity profile in the liquid and solid vortex phases is resolved providing information about the transverse dynamic correlation of vortices. While in the liquid phase the vortices respond locally to the driving force, in the solid regime they show long range velocity correlation over macroscopic distances. At high driving force gradients, vortex-vortex shear stresses exceed the elastic limit and the dynamics is characterized by plastic motion. [S0031-9007(98)08260-X]

PACS numbers: 74.60.Ge, 74.25.Fy

The magnetic field in superconductors is carried by an array of discrete flexible vortex lines [1] which transform into solid, liquid, and glassy phases [2] depending on their density and temperature, much like the analogous phases of ordinary matter. The dynamic response of these vortex line phases determines the electrodynamic behavior of superconductors and is a central subject of scientific and practical interest. On the practical side, the dissipation caused by vortex motion restricts the performance of bulk and thin film superconducting devices in a variety of applications. On the scientific side, information about vortex-vortex interactions and their dynamics [3–5] is essential to any theory describing vortex matter.

In this paper we report transport experiments in a contact configuration that allows measurement of transverse vortex-vortex velocity correlations. We employ an unconventional circular geometry to impose a controlled driving force gradient on the vortices and spatially resolve their transverse velocity correlation. We find that the velocity in the liquid state responds locally to the driving force with no evidence for long range velocity correlation. Remarkably, the vortex solid phase shows a highly nonlocal velocity response over macroscopic length scales which implies rigid rotation of the vortex lattice. At high driving gradients the rotating lattice shears along concentric circles to form rigidly rotating rings.

The experimental arrangement is shown in Fig. 1. Untwinned crystals of $YBa_2Cu_3O_{7-\delta}$ were cleaved into two pieces—one piece carefully polished into a disk shape and the other into a rectangular geometry commonly used in four-probe resistivity measurements. Current is injected at the center of the disk and removed at the perimeter (Fig. 1a) to induce a radial current density J that decays as $1/r$ (Fig. 1b). Our samples are approximately 700 μm in diameter with thicknesses of less than 10 μm to ensure a uniform current distribution along the c axis [6]. For flux lines parallel to the disk axis, the radial current induces an azimuthal Lorentz force falling off as $1/r$. In the absence of in-plane vortex-vortex velocity correlation each vortex moves independently with a radial velocity

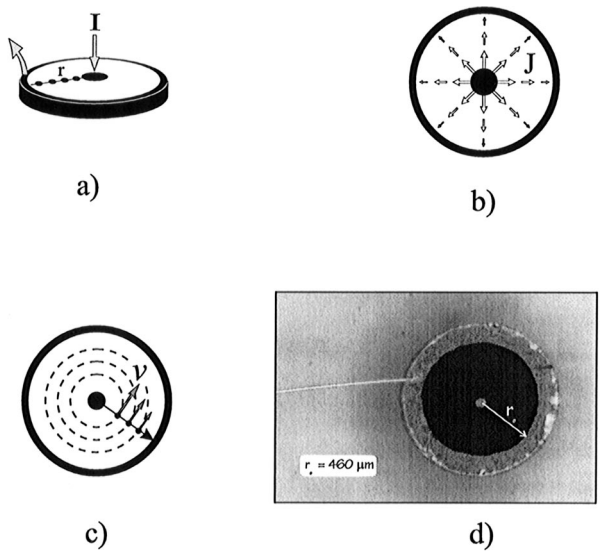

FIG. 1. Contact and sample geometry used in our transport measurements. In a superconducting crystal polished as a circular disk an in-plane nonuniform radial current distribution is induced. Application of a current at the central gold contact and removal at the perimeter of the disk (a) produces a radial current density J falling off as $1/r$ (b). Vortex lines perpendicular to the disk plane experience a Lorentz force perpendicular to the radius r and move in concentric orbits with velocities $v(r)$. In the absence of transverse vortex-vortex correlation, the vortices near the center move faster than those near the perimeter (c) according to $v(r) \sim J \sim 1/r$. The radial dependence of the vortex velocity is given by the voltage profile sampled by the probes located along a radius (a). (d) Photograph of one of the samples used in the experiment.

dependence $v \sim J \sim 1/r$ (Fig. 1c). However, if over some length scale the in-plane vortex motion is correlated, we should detect a deviation from the $1/r$ velocity distribution. To spatially resolve the radial dependence of the vortex velocity and the length scale of the vortex-vortex correlation, we evaporated a series of voltage contacts along a radius at 60 μm intervals (Fig. 1a). Figure 1d shows a photograph of one of the samples used here.

The resistance of the normal state and the driven dynamics of the vortex liquid state are shown in the upper panel of Fig. 2. The resistance derived from adjacent pairs of voltage contacts falls off with radius, $R_{12} > R_{23} > R_{34}$. In the normal state, this reflects the current density distribution, which decreases with increasing radius. In contrast, in the vortex liquid regime between T_c and T_m, the resistance is a measure of the vortex velocity. The data show that vortices near the center, where the current density and driving force are larger, move faster than those near the perimeter. The resistance in the normal and vortex liquid regimes can be collapsed to a single curve using a simple scaling law based on linear resistivity and a $1/r$ current density [7–9]. The voltage difference between contact n and $n + 1$ is given by

$$V_{n,n+1} = \int_n^{n+1} E\, dr = \frac{\rho I}{2\pi d} \ln\left(\frac{r_n}{r_{n+1}}\right), \qquad (1)$$

where E is the electric field, ρ is the resistivity, I is the applied current, d is the sample thickness, and r_n is the radial position of the nth contact. The lower panel of Fig. 2 shows the resistivity derived from Eq. (1) using the data of Fig. 2a. In the normal state this scaling proves the $1/r$ distribution of the current density. Remarkably, the same scaling applies to the vortex liquid regime. This shows that each vortex responds locally to the $1/r$ driving force without correlation over the length scale of our experiment. The onset of the sharp drop in the resistivity at T_m, indicative of the first order vortex melting transition [10–16], remains independent of the current density and vortex velocity gradients in our experiment.

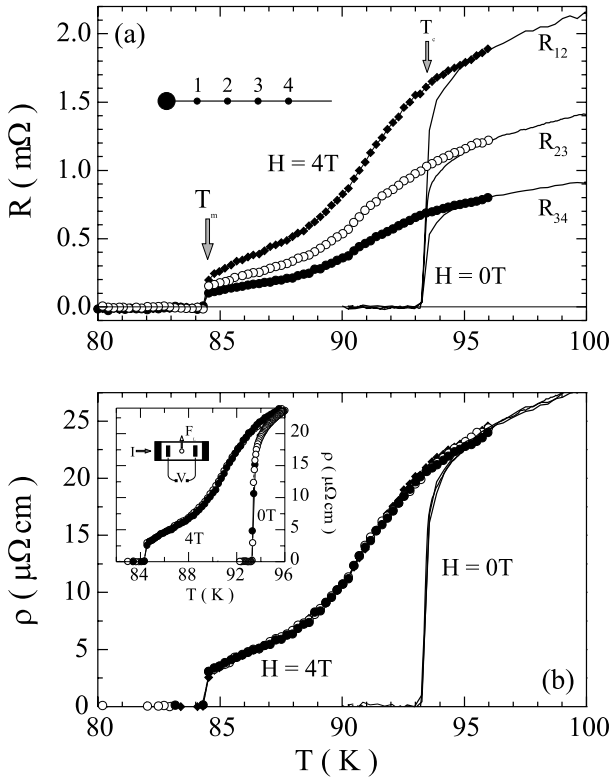

FIG. 2. (a) Temperature dependence of the resistance measured between adjacent contacts for 0 and 4 T applied magnetic field. The voltage probes are numbered sequentially from the center of the disk (see inset). Symbols: ◆: R_{12}; ○: R_{23}; ●: R_{34}. (b) Resistivity versus temperature obtained using the data shown in (a) and Eq. (1) (see text). The inset compares the resistivity obtained from contacts 3 and 4 with that of a slab shaped sample where vortices enter and exit the sample.

The role of the surface barriers [17,18] in the liquid state dynamics is shown by comparison of the resistivity derived from the circular and rectangular geometries. In the circular geometry the vortices move in concentric orbits and do not enter or exit the sample. The measured resistivity is therefore independent of surface effects. The inset in Fig. 2b shows the data for the circular and rectangular sample at 4 T. The two curves are nearly identical, demonstrating that our measured resistivities in both the rectangular and circular samples represent bulk rather than surface behavior.

Unlike the vortex liquid, the solid exhibits dramatic velocity correlations. Figure 3a shows the resistivity for adjacent voltage probes in the vicinity of the vortex solid-liquid phase transition for two different driving currents. The square symbols correspond to an applied current of 0.5 mA and clearly show the onset of the drop in the resistance at T_m (dotted line). Below this temperature, a finite critical current is detected and the resistance is a nonlinear function of the current. For high nonuniform driving forces ($I = 15$ mA in Fig. 3a) the resistances decrease continuously with temperature and cross in pairs near the temperature T_{cross}. Below T_{cross} the resistance curves reverse their relative values, i.e., $R_{12} < R_{23} < R_{34}$, indicating that the vortices near the center move more slowly than those at the perimeter, contrary to the driving force distribution. This behavior is opposite to that in the liquid. T_{cross} is current dependent and extrapolates to T_m in the limit of zero current.

The simplest structure that will give a radially increasing resistance is a vortex lattice rotating as a rigid body with the angular velocity ω. In this case the vortices move with velocity $v(r) = \omega r$ with $\omega = \omega(T, I)$. This velocity distribution implies a scaling quite different from that of the liquid [Eq. (1)]. In rigid rotation, the voltage drop between adjacent contacts is given by

$$V_{n,n+1} = \int_n^{n+1} E\, dr = \frac{B}{2}(r_{n+1}^2 - r_n^2)\omega(T, I). \qquad (2)$$

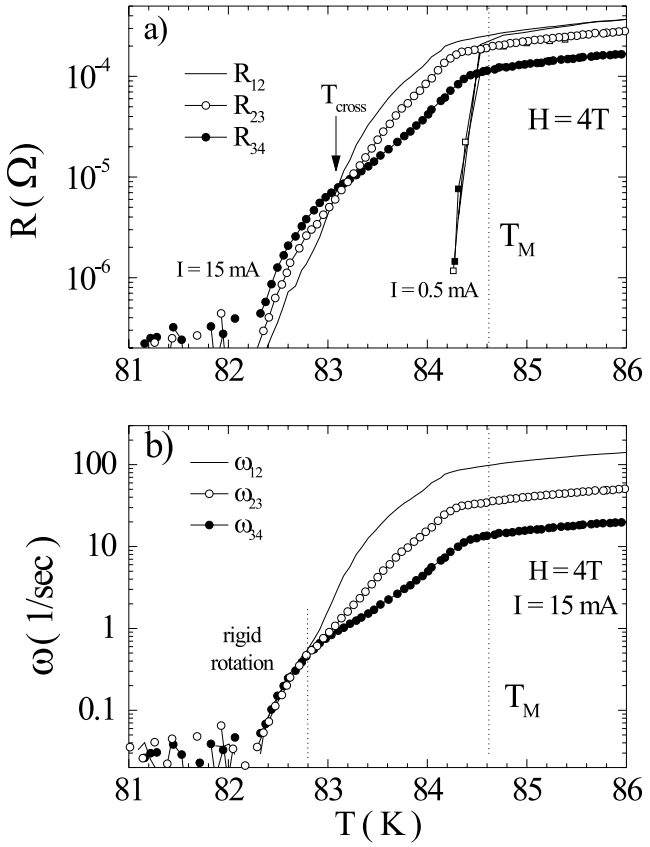

FIG. 3. (a) Resistivity for adjacent voltage probes in the solid vortex phase ($T < T_m$) for fixed magnetic field and different applied currents. (b) Temperature dependence of the angular velocity ω of the rotating vortex solid. The angular velocity was obtained from the data of (a) and Eq. (2). The temperature interval where rigid rotation is detected is indicated.

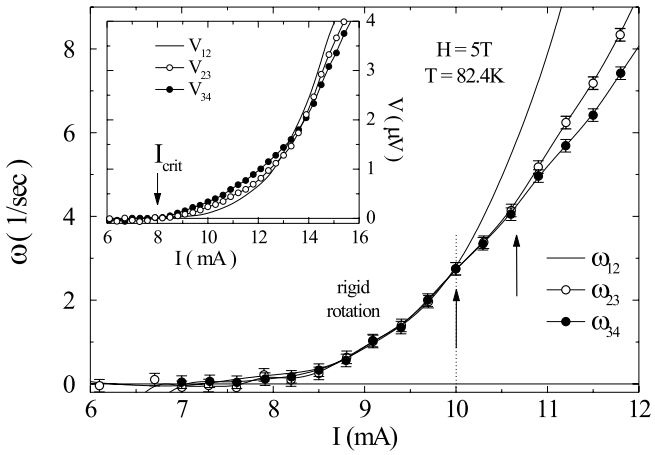

FIG. 4. Current dependence of the angular velocity in the vortex solid phase. The I-V data shown in the inset together with Eq. (2) were used to obtain $\omega(I)$ (main panel). The arrows indicate the current above which the rigid rotation breaks down.

Using Eq. (2) we can extract the temperature and current dependence of ω. Figure 3b shows $\omega(T)$ obtained from the low temperature data of Fig. 3a. The scaling of the data shows that the vortex lattice rotates as a rigid body over macroscopic length scales. The in-plane vortex correlation extends up to the size of the sample, of order 10^4 vortex lattice spacings. At higher temperature, approaching the melting temperature, the vortex lattice softens and rigid body motion can no longer be sustained.

The details of the depinning process and the rigid rotation dynamics are revealed by the I-V curves at low temperature (inset in Fig. 4). Figure 4 shows the current dependence of the angular velocity ω derived from the I-V curves shown in the inset. Within our resolution, we find a position independent critical current $I_{\rm crit}$ consistent with the onset of rigid rotation. Above $I_{\rm crit}$ the vortices begin to move coherently indicating elastic depinning of the vortex lattice. For a limited range of currents above $I_{\rm crit}$ the lattice rotates as a rigid body, $\omega_{12} = \omega_{23} = \omega_{34}$. The maximum rotation speed in this range is $\omega \sim 3\ \mathrm{sec}^{-1}$, about one turn in 2 sec. At higher currents a shear-induced breakdown of rigid rotation scaling is observed. Figure 4 shows that the breakdown first occurs near the center of the sample when ω_{12} rises above ω_{23} and ω_{34}. The relative angular velocities $\omega_{12} > \omega_{23} = \omega_{34}$ indicate that the sample has sheared into rings, with the inner portion rotating faster than the outer ring which continues to rotate rigidly. The faster rotation of the inner ring is consistent with the larger driving force at smaller radii. At higher driving forces and force gradients, the rigid rotation of the outer ring is broken as $\omega_{23} > \omega_{34}$.

At temperatures between T_M and the onset of rigid rotation (Fig. 3b) or at high drive (Fig. 4), neither the liquid ($v \sim 1/r$) nor the rigid rotation ($v \sim r$) scaling is observed. Here we see the development of plastic motion characterized by vortex-vortex velocity correlations which are intermediate between those of the liquid and lattice. As in crystalline solids, the rigidity of a magnetic flux line lattice collapses due to melting or high shear stress.

Our experiments with circular vortex motion in the presence of a controlled force gradient demonstrate a new approach to measuring the dynamic response of the liquid and solid vortex phases. The control of the driving force gradient and the measurement of the spatial dependence of the velocity response are a uniquely powerful combination for measuring such basic properties as the shear modulus of the solid, the shear viscosity of the liquid, and the nature of plastic motion.

We thank David Nelson, Christina Marchetti, David Huse, Stefan Scheidl, and Alex Koshelev for valuable discussions. This work was supported by the U.S. Department of Energy, Office of Basic Energy Sciences-Material Sciences under Contract No. W-31-109-ENG-38 (W. K. K., R. J. O., A. P., G. W. C.), the National Science Foundation through the Science and Technology Center for Superconductivity under Contract No. DMR91-20000 (D. L.), and Division of Materials Science under Contract No. DMR-9702535 (H. S.). L. M. P. acknowledges

support from the U.S. Department of Energy administered through the Division of Educations Programs of Argonne National Laboratory.

[1] A. A. Abrikosov, Zh. Eksp. Teor. Fiz. **32**, 1442 (1957) [Sov. Phys. JETP **5**, 1174 (1957)].
[2] George W. Crabtree and David R. Nelson, Phys. Today **50**, No. 4, 38 (1997), and references therein.
[3] M. C. Marchetti and David Nelson, Phys. Rev. B **42**, 9938 (1990).
[4] R. Wortis and D. A. Huse, Phys. Rev. B **54**, 12 413 (1996).
[5] M. H. Theunissen, E. Van der Drift, and P. H. Kes, Phys. Rev. Lett. **77**, 159 (1996).
[6] D. Lopez, E. F. Righi, G. Nieva, F. de la Cruz, W. K. Kwok, J. A. Fendrich, G. W. Crabtree, and L. Paulius, Phys. Rev. B **53**, 8895 (1996).
[7] S. A. Sergeenkov, V. V. Gridin, and M. Ausloos, Z. Phys. B **101**, 565 (1996).
[8] M. P. Shaw and P. R. Solomon, Phys. Rev. **164**, 535 (1967).
[9] R. P. Huebener, *Magnetic Flux Structures in Superconductors* (Springer-Verlag, Berlin, 1979).
[10] H. Safar, P. L. Gammel, D. A. Huse, D. J. Bishop, J. P. Rice, and D. Ginsberg, Phys. Rev. Lett. **69**, 824 (1992).
[11] W. K. Kwok, S. Fleshler, U. Welp, V. M. Vinokur, J. Downey, G. W. Crabtree, and M. M. Miller, Phys. Rev. Lett. **69**, 3370 (1992).
[12] M. Charalambous, J. Chaussy, and P. Lejay, Phys. Rev. B **45**, 5091–5094 (1992).
[13] R. Liang, D. A. Bonn, and W. N. Hardy, Phys. Rev. Lett. **76**, 835 (1996).
[14] U. Welp, J. A. Fendrich, W. K. Kwok, G. W. Crabtree, and B. W. Veal, Phys. Rev. Lett. **76**, 4809 (1996).
[15] J. A. Fendrich, U. Welp, W. K. Kwok, A. E. Koshelev, G. W. Crabtree, and B. W. Veal, Phys. Rev. Lett. **77**, 2073 (1996).
[16] A. Schilling, R. A. Fisher, N. E. Phillips, U. Welp, W. K. Kwok, and G. W. Crabtree, Nature (London) **382**, 791 (1996).
[17] C. P. Bean and J. D. Livingston, Phys. Rev. Lett. **12**, 14 (1964).
[18] D. T. Fuchs, E. Zeldov, M. Rappaport, T. Tamegai, S. Ooi, and H. Shtrikman, Nature (London) **391**, 373 (1998).